Fractographic Analysis of the Low Energy Fracture of an Aluminum Alloy

by

J. Tanaka, C. A. Pampillo and J. R. Low, Jr.

Metallurgy & Materials Science
Carnegie-Mellon University
Pittsburgh, Pennsylvania 15213

METALS RESEARCH LABORATORY
CARNEGIE INSTITUTE OF TECHNOLOGY

Carnegie-Mellon University

PITTSBURGH, PENNSYLVANIA

National Aeronautics and Space Administration
Research Grant NGR 39-087-300

Fractographic Analysis of the Low Energy Fracture of an Aluminum Alloy

by

J. Tanaka, C. A. Pampillo and J. R. Low, Jr.

Metallurgy & Materials Science
Carnegie-Mellon University
Pittsburgh, Pennsylvania 15213

NASA Technical Report No. 1

This investigation was made possible by a Research Grant from the National Aeronautics and Space Administration

INTRODUCTION

The brittle fracture of many so-called high strength aluminum, titanium and iron-base alloys has been shown to occur by dimpled rupture[1]. This mode of fracture, as contrasted, for example, with the cleavage mode, is normally associated with ductile materials and various studies have shown that the fracture process is, generally: nucleation of voids at impurity particles and the growth and coalescence of these voids during plastic deformation to produce final rupture. These observations on ductile materials suggest that the fracture toughness of the more brittle, high strength materials, may be strongly affected by the density and distribution of impurity particles which do not contribute to the strength. For this reason a study of the fracture process in a high strength aluminum alloy (2014T6) was undertaken to identify the void nucleating particles in this material, to determine their composition, and to suggest means by which they might be eliminated without loss of strength.

MATERIAL

A two inch thick plate of commercial 2014 aluminum alloy, heat treated to the T6 condition, was used to make specimens for fracture testing. The chemical composition and tensile data of the alloy are listed in Tables I and II.

Table I

Composition of 2014 Al-Cu Alloy (wt. pct.)

	Cu	Si	Mn	Mg	Fe	Al	Upper Limits
Composition Limits	3.9 ~5.0	0.5 ~1.2	0.4 ~1.2	0.2 ~0.8	0.7 Max.	Rem	Ti-0.15 Zn-0.25 Cr-0.10
Actual Analysis	4.64 4.71	0.84 0.81	0.72 0.73	0.51 0.51	0.2 0.2		

Table II

Typical Mechanical Properties of 2014-T6 Alloy

Yield Strength psi	Tensile Strength psi	Elongation in 2" (%)
60,000	68,000	10

Fracture toughness tests were made at the NASA Lewis Research Center by W. F. Brown and J. E. Srawley. Figure 1 shows the shape and dimensions of the fatigue-cracked toughness specimens. Toughness measurements were all made in the "TR" testing direction, i.e. the fracture surface lies perpendicular to the thickness of the plate and the crack propagation direction is parallel to the rolling direction. A mean value, of six tests, of K_{Ic} = 17.6 KSI$\sqrt{in.}$ ±0.4 KSI$\sqrt{in.}$ was obtained. This value may be considered rather low compared, for instance, with the values obtained at equal yield stress for other aluminum alloys, for which K_{Ic} is around 30 KSI$\sqrt{in.}$ [1].

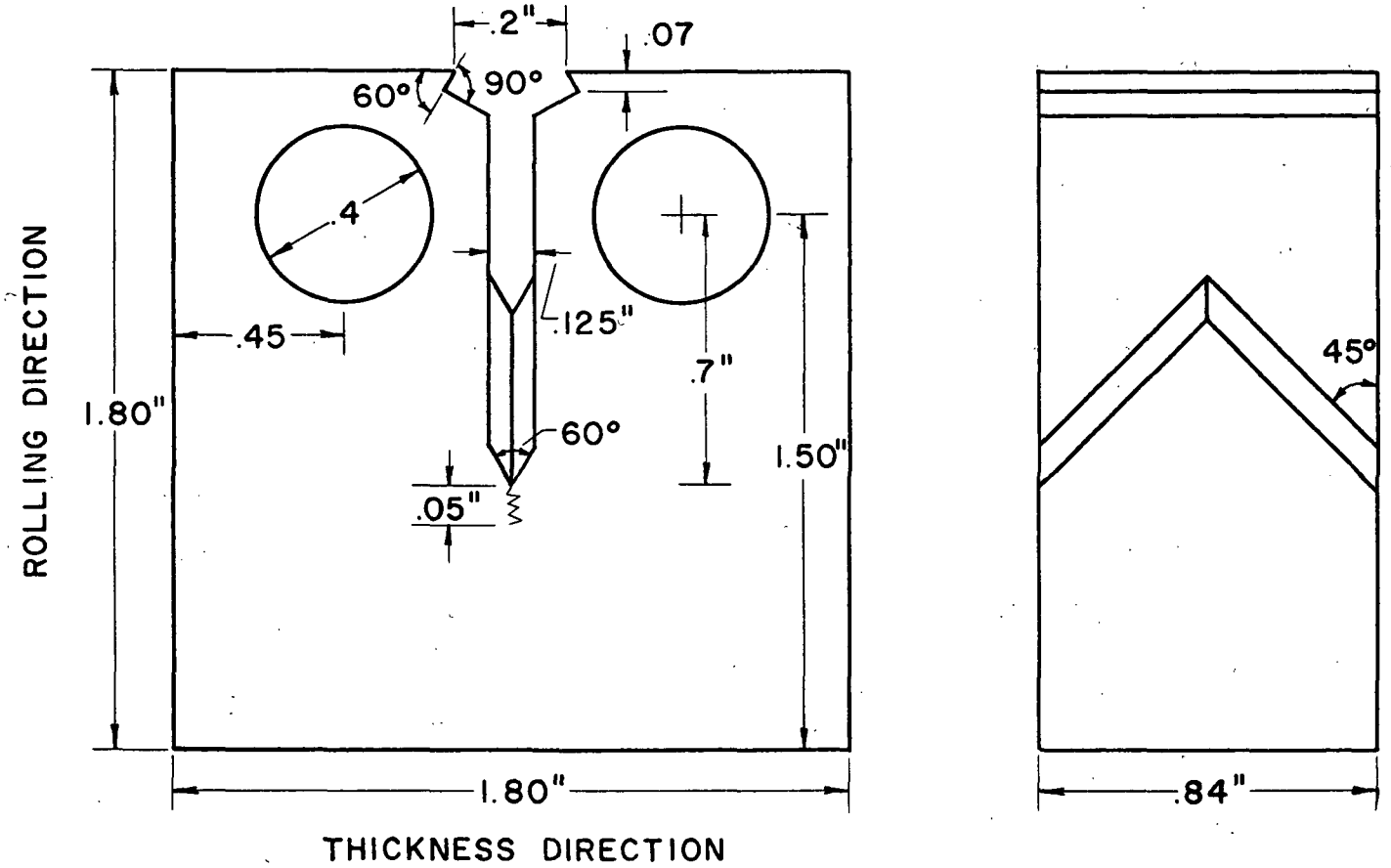

Fig. 1 Compact Fracture Toughness Specimen

FRACTOGRAPHIC STUDY

Two techniques were used to study the fracture surfaces of the cracked specimens. One was the observation with the electron microscope, of two stage plastic-carbon replicas of the fracture surface; and the other was direct observation of these surfaces with the scanning electron microscope.

a. Replicas

Figures 2 and 3 show typical electron microscope fractographs. A dimpled topography was found over the entire fracture area observed. The most salient feature to be noted here, is that two widely different sizes of dimples are present; moreover, they are not randomly distributed but form groups, or colonies, of large (10 to 30 microns) dimples (A) separated from similar areas by bands of small (0.5 to 2 microns) dimples (B). In some areas of some of the large dimples, features typical of a cleavage pattern, (C) are observed. These are thought to be due to the fracture of an inclusion which failed by cleavage and nucleated the void. The greater proportion (50-60%) of the fracture surface is covered by large dimples and it is very likely, then, that the most important factor leading to the low toughness of the alloy is the existence of the particles which nucleate the large size dimples.

b. Scanning Electron Microscopy

Although of lower resolution than the transmission electron microscope, the scanning electron microscope (SEM) allows the direct observation of the fracture surfaces and also observations at much lower magnifications of areas that can then be magnified extensively for more detailed study. This allows the observer to relate the submicroscopic features seen at high magnifications to the grosser features of the fracture surfaces.

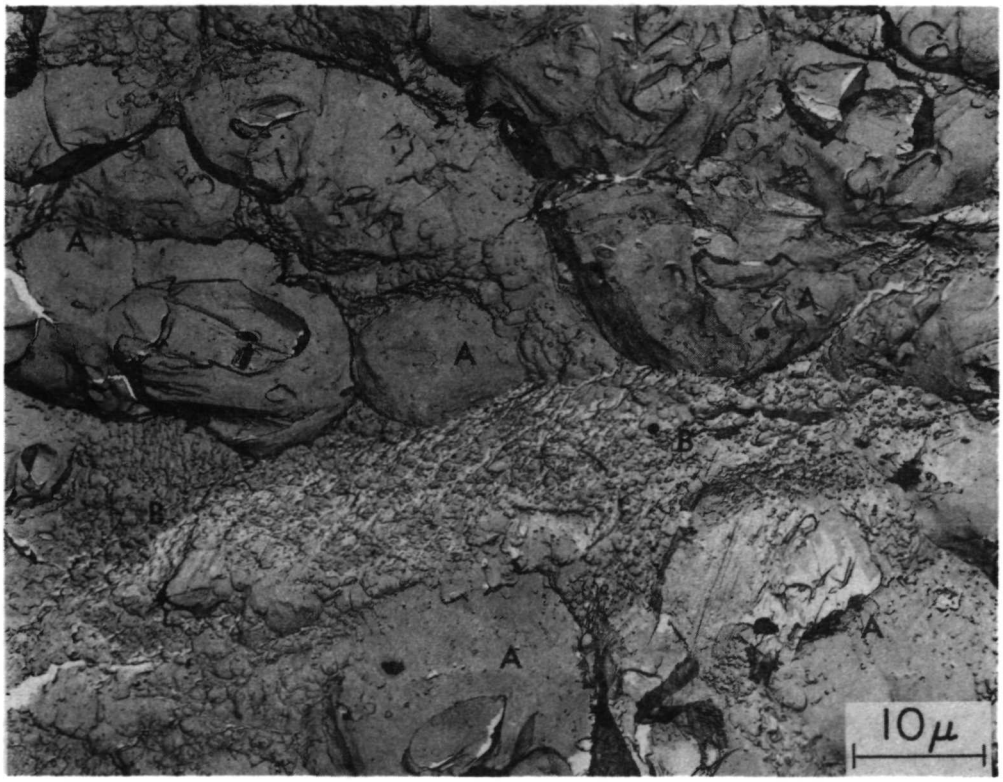

Figures 2 and 3 Two Stage Plastic-carbon Replica of Fracture Surface. Large Dimples at A - Small Dimples at B - Cleavage Pattern at C

Figure 4 shows a low magnification fractograph taken with the SEM of the fracture surface of one of the toughness specimens. By careful examination it is possible to distinguish areas with the same large dimples seen in the replicas and smoother areas which at higher magnifications, Figures 5 and 6, show the topography of the small dimples. "A" marks the same point in the three micrographs of Figures 4, 5 and 6. All these micrographs were taken with secondary electrons. Figures 7 and 8 compare, at low magnification, the same area taken with secondary electrons and with back scattered electrons. When back scattered electrons are used, deep shadows appear where secondary electrons showed areas of small dimples (smooth at low magnifications). This means that these areas of small dimples are steps on the fracture surfaces joining areas covered by large dimples that lie at different levels (back scattered electrons give an effect similar to highly oblique light in the optical microscope). The reason why these areas did not appear as steps on the fractographs obtained by replicas is that these steps are too large and the replicas probably collapse, showing large size and small size dimples at the same level. (See Figures 2 and 3)

FAILURE OF LARGE INCLUSIONS

Figure 9 shows an optical micrograph of a mechanically polished section of the material. Large inclusions, 3 to 10 microns in diameter, separated by a distance of 5 to 15 microns from each other, may be seen. In some cases, grouping of these inclusions into colonies were observed, but the general distribution was quite uniform except for a certain tendency of the inclusions to be aligned along the rolling direction (marked as R in Fig. 9).

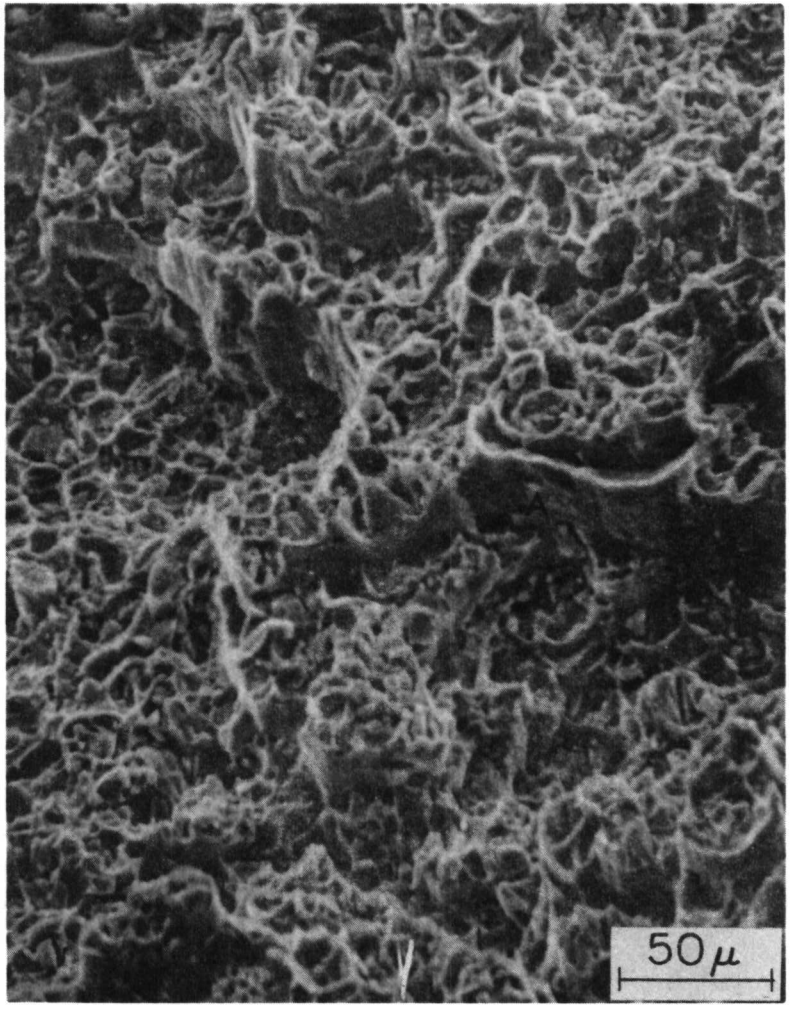

Fig. 4 Scanning Electron Microscope Micrograph Showing Large Dimples and Smoother Areas at A (secondary electrons).

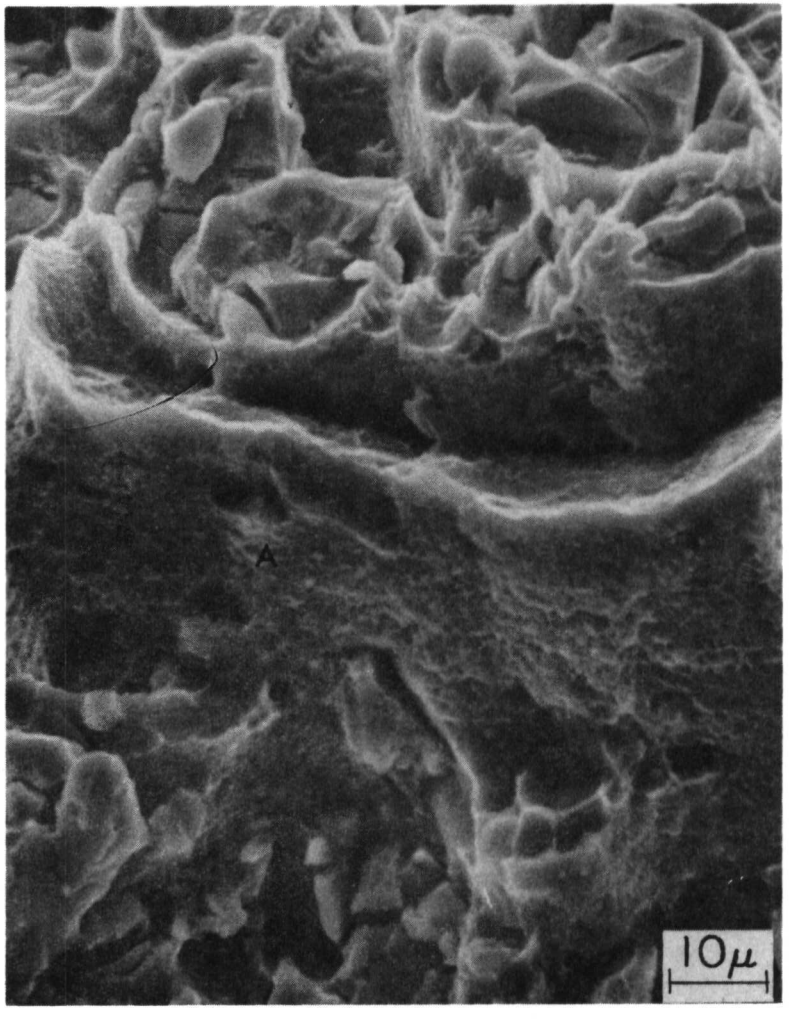

Fig. 5 Same as Fig. 4 at Larger Magnification (secondary electrons) A is the Same Spot as in Fig. 4

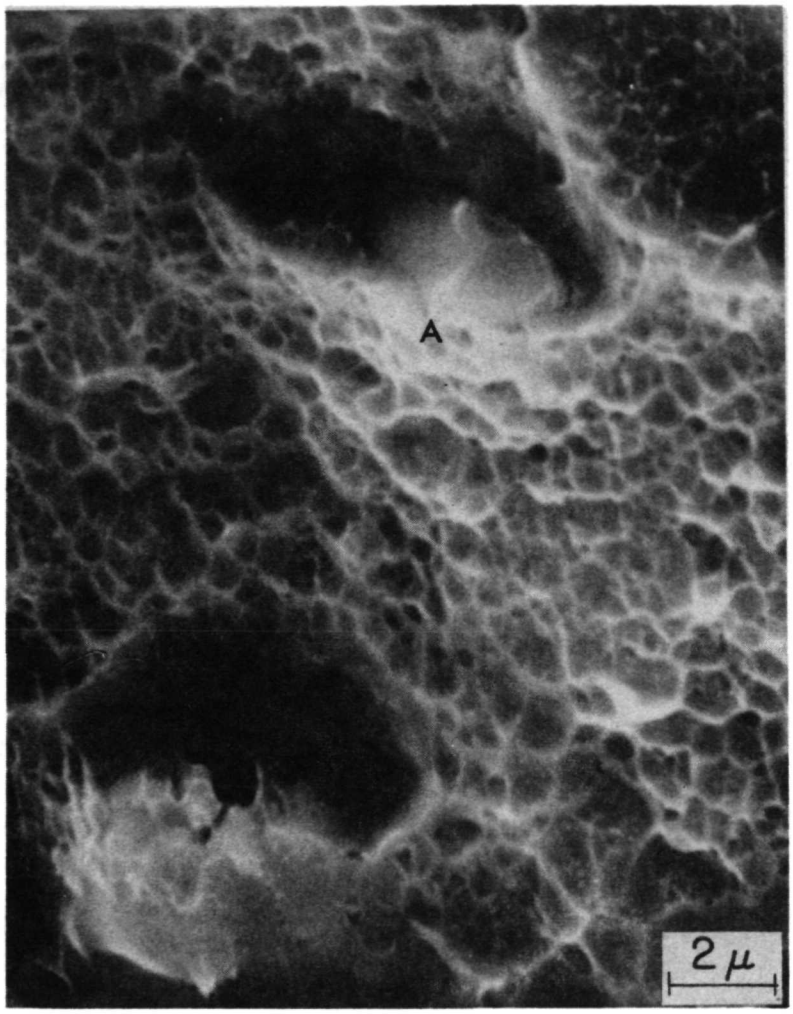

Fig. 6 Same as Fig. 4 and 5 at Higher Magnification Showing Small Dimples on Smoother Areas of Fig. 4 (secondary electrons) A is the Same Spot as in Figs. 4 and 5

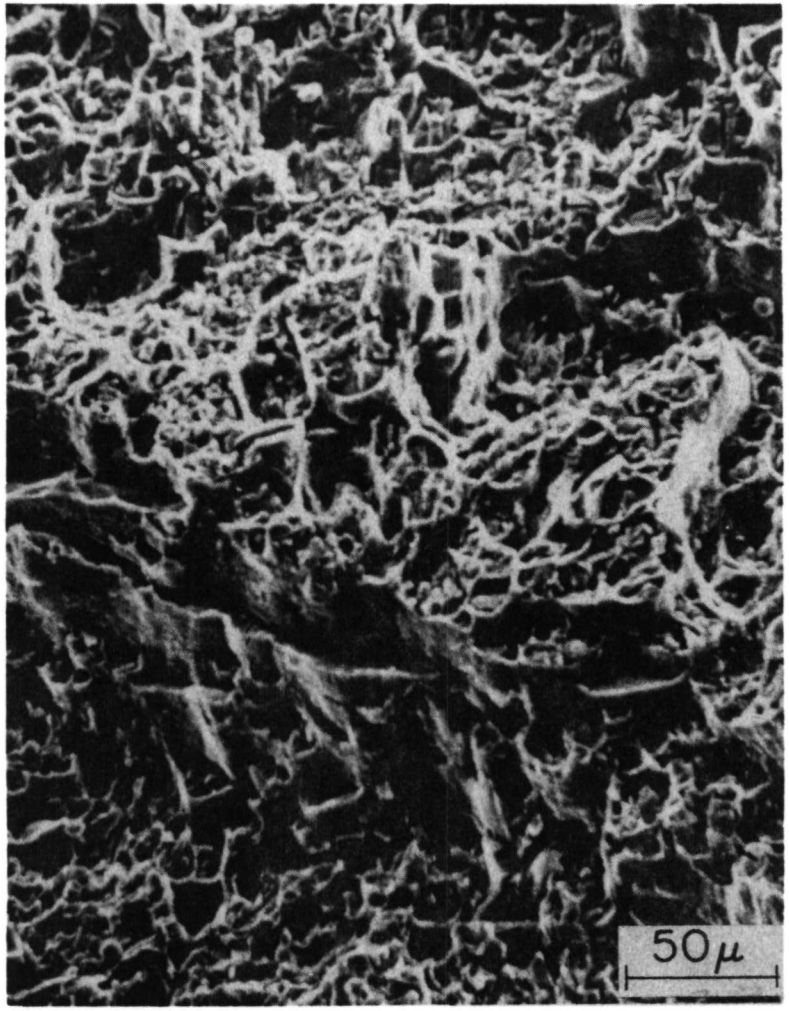

Fig. 7 Low Magnification Scanning Electron Micrograph Taken with Secondary Electrons, to Compare with Back Scattered Electrons in Fig. 8

Fig. 8 Same as Fig. 7 Taken with Back Scattered Electrons

Two types of inclusions may be distinguished, by their shape and color in the optical microscope. One with a more rounded shape appears yellowish under the microscope (clear grey in the micrographs) and the other of a more irregular form appears as a darker yellow (darker grey in the micrographs).

A preliminary experiment was made to study the nucleation of cracks in the alloy by bending prepolished samples in a three point bending jig. This method of deforming the sample was changed later to tensile deformation in an Instron machine, because it was found that the preparation by polishing seemed to disturb the particle matrix interface leading to incorrect conclusions about the mode of failure of the inclusions. However, one valid result obtained was that after a significant amount of deformation at the bent surface, short cracks appeared which were not related to the inclusions. By slightly etching the surface with Kellers reagent (0.5HF, 1.5Cl, 2.5HNO_3 95H_2O) it was found that these cracks were located at grain boundaries as shown in Figure 10 by arrows. These cracks did not grow to produce total fracture and further deformation resulted in sudden fracture of the specimen. Its fracture surface presented the typical dimpled topography, already shown, with no clear evidence of intergranular failure.

Further experiments, which we believe clearly show the nucleation of the fracture process, were made by observations of polished surfaces of tensile samples deformed in tension by different amounts in an Instron machine. After deformation, the specimens were cut at mid thickness parallel to the tensile axis and mechanically polished very carefully with metallographic papers through the 0000 grade and finally lapped with a MgO powder as the abrasive. Two polished surfaces were observed, one corresponding to the

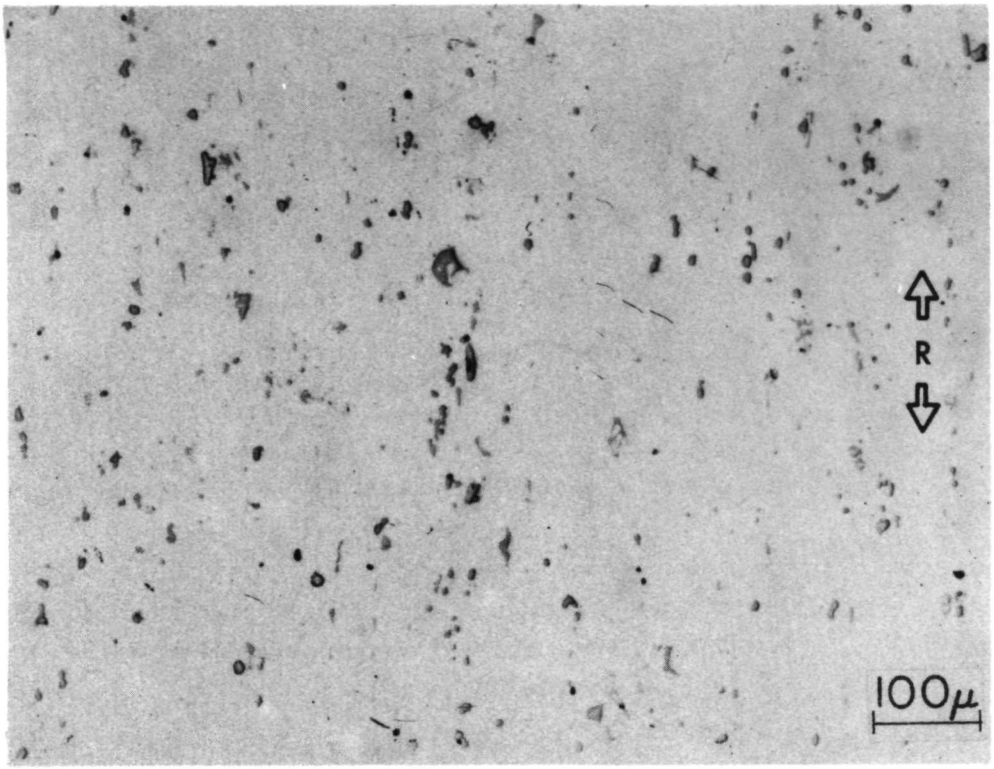

Fig. 9 Optical Micrograph of a Mechanically Polished Surface of the Alloy

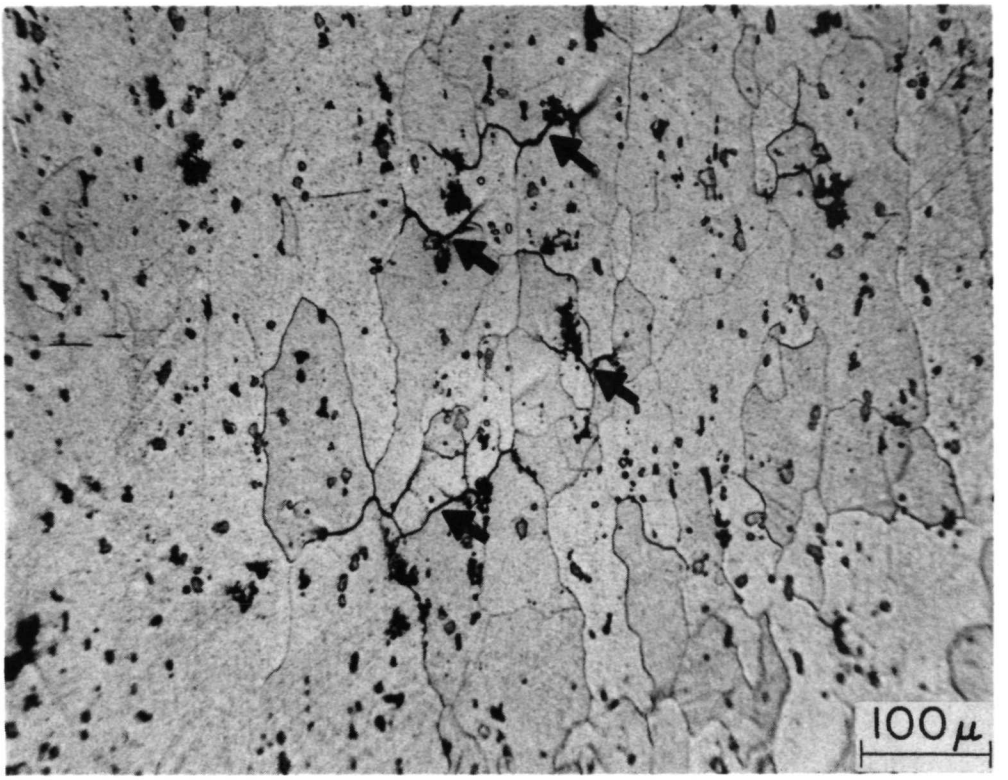

Fig. 10 Optical Micrograph. The Polished Surface was Etched to Delineate Grain Boundaries After Cracks (arrows) had Appeared as a Result of Bending Deformation

mid section and the other to the free surface of the specimen. The ratio of cracked particles to the total number of particles greater than 1 micron in diameter, is shown in Figure 11 as a function of deformation. The solid circles correspond to the observations made at the free surface and the open circles at the mid section. It is clear that the particles start cracking at the early stages of deformation. The fraction of cracked inclusions increases steadily up to a point where the maximum load is reached, after which the rate of cracking increases sharply.

Initially it was not clear if the deformation to reach maximum load was due to the cracking of the particles or if the rate of cracking of particles increased because this deformation has been reached. A rough estimate of the load bearing area of the particles, which is about 1 to 2% of the total area of the sample, seems to point to the latter as the most likely possibility. It is interesting to note that the fraction of cracked particles at the free surface is larger for strains smaller than the necking strain than the same fraction measured at the mid section.

The cracks formed at the inclusions were only seen to propagate into the matrix for the largest deformations and this was observed more frequently at the mid section, Figure 12 (S shows the stress direction). Blunting of the cracks formed at the inclusions were observed in some cases and this was due to failure at the particle matrix interface, as shown in Figure 13 by arrows. Some evidence of grain boundary cracking is found in specimens with the larger deformations. This is shown in Figure 14 by arrows. The different appearance of the crack as compared with that in Figure 10 is believed to be due to rounding of the edges by polishing.

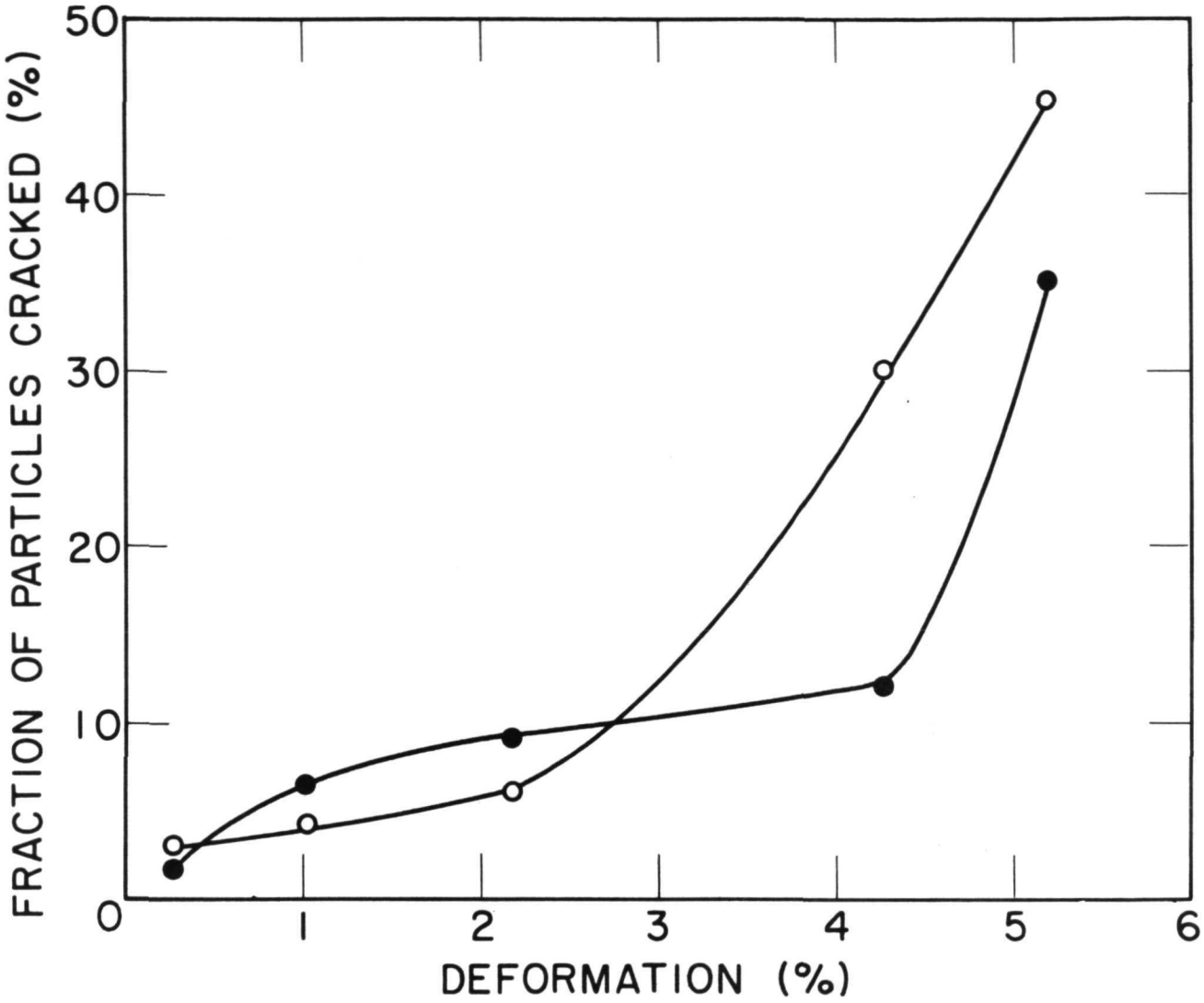

Fig. 11 Fraction of the Inclusions Greater than 1 Micron Found Cracked as a Function of Tensile Plastic Deformation. Solid Circles Correspond to Observations Made at the Free Surface of the Specimen and Open Circles at the Mid Section

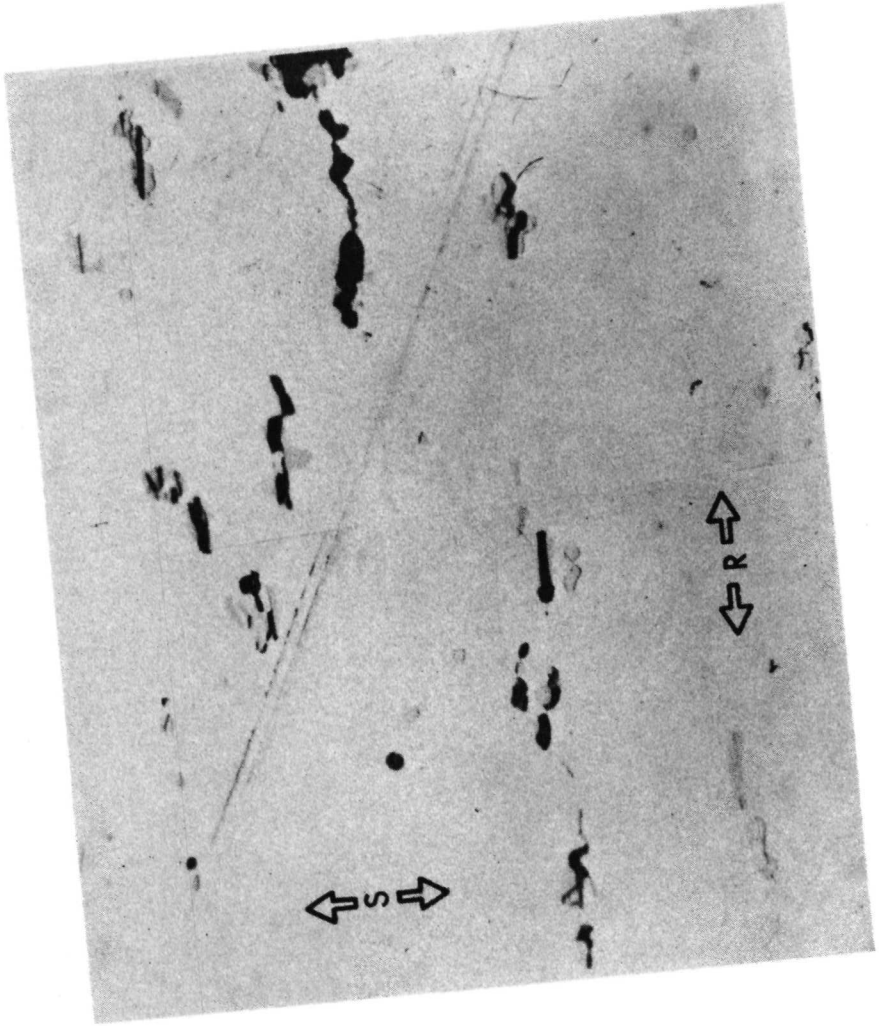

Fig. 12 Polished Surface of Fractured Tensile Specimen Showing Growth of Cracks. S is the Tensile Axis and R the Rolling Direction

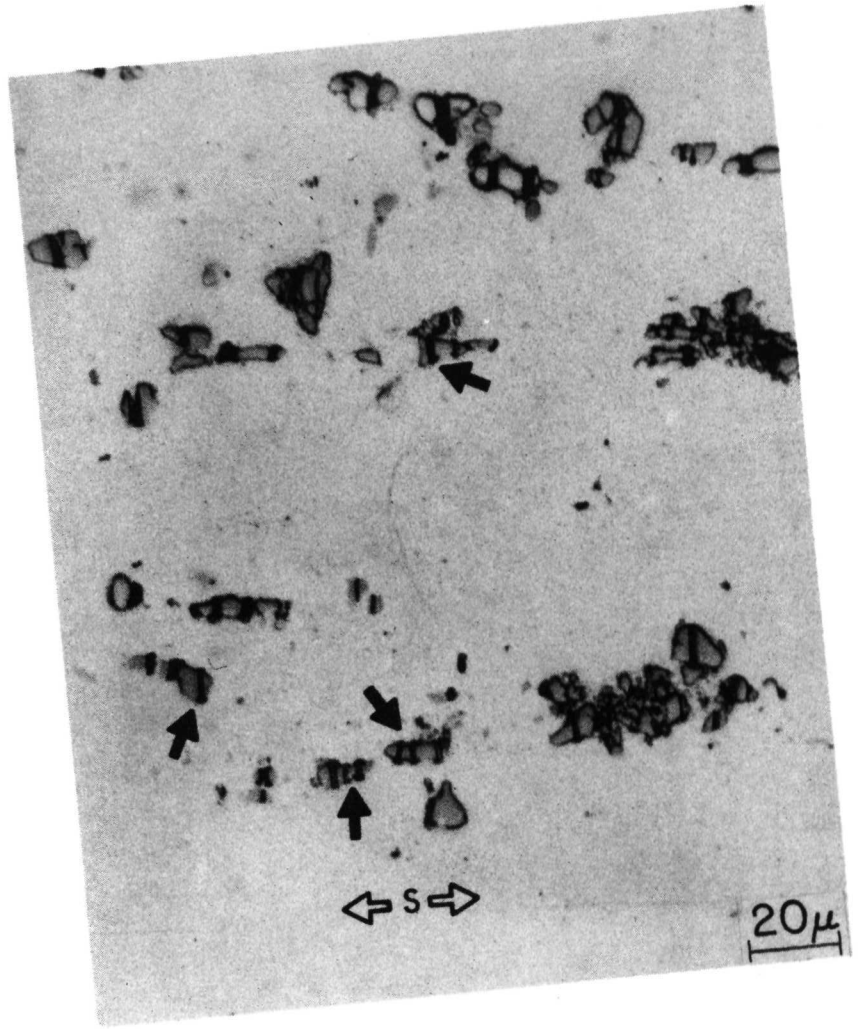

Fig. 13 Polished Surface of Tensile Specimen Showing Blunting of the Cracks in the Inclusions (arrows). S is the Tensile Axis

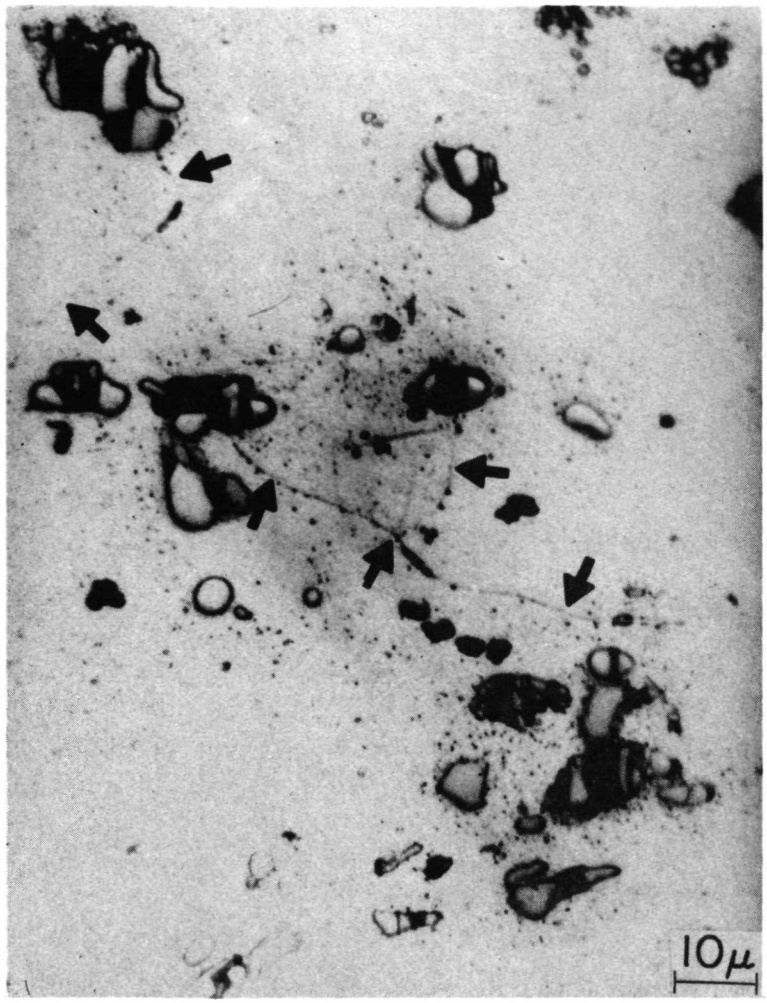

Fig. 14 Polished Surface of Tensile Specimen Showing Grain Boundary Cracking (arrows)

TRANSMISSION ELECTRON MICROSCOPY

The small size dimples seen on the fracture surfaces were very likely nucleated at particles too small to be observed with the optical microscope. Moreover the observation that some in grain boundary cracking occurred without showing typical intergranular fracture appearance in the fractographs, suggested that a precipitation free zone around grain boundaries might exist in the alloy. This is known to lead, in some cases, to grain boundary failure with a dimpled fracture topography[2]. With this in mind, thin films of the alloy were examined in the electron microscope. The thin films were prepared by a jet electropolishing technique[3] using a mixture of 2/3 Methanol and 1/3 Nitric Acid. Figure 15 shows a typical transmission electron micrograph. Small particles about 0.1 to 0.2 microns in diameter a distance of about 0.5 to 1 micron apart are clearly seen. Because of their size and distribution, these should be regarded as a dispersion which strengthens the matrix. The work hardening characteristics of the alloy should be especially affected by them[4]. This coarse dispersoid, which contributes significantly to the strength of the alloy in addition to the fine θ' precipitate, has been identified as $Al_{12}(Mn, Fe)_3 Si$[8].

At higher magnifications, Figure 16, the matrix shows a structure formed by a fine elongated precipitates 0.01 to 0.05 microns long which are believed to be the principal hardening precipitates. No precipitation free zone was found around grain boundaries but elongated inclusions 0.3 to 0.5 microns long were observed, Figure 17. This finding may well explain the grain boundary cracking observed in the bending and tensile specimens. The fact that the fracture topography was of the dimple type and did not show any evidence of grain boundary interface failures may also be understood. In effect, the existence of grain boundary failure showing a dimpled topography

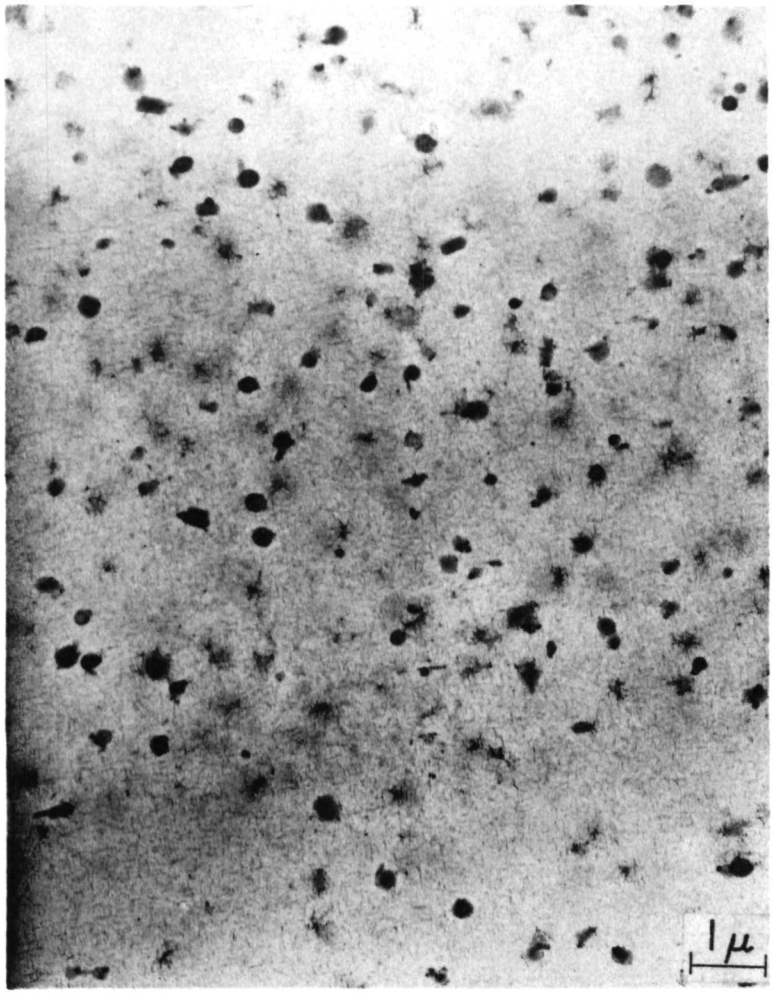

Fig. 15 Transmission Electron Micrographs Showing a Fine Dispersion of Particles

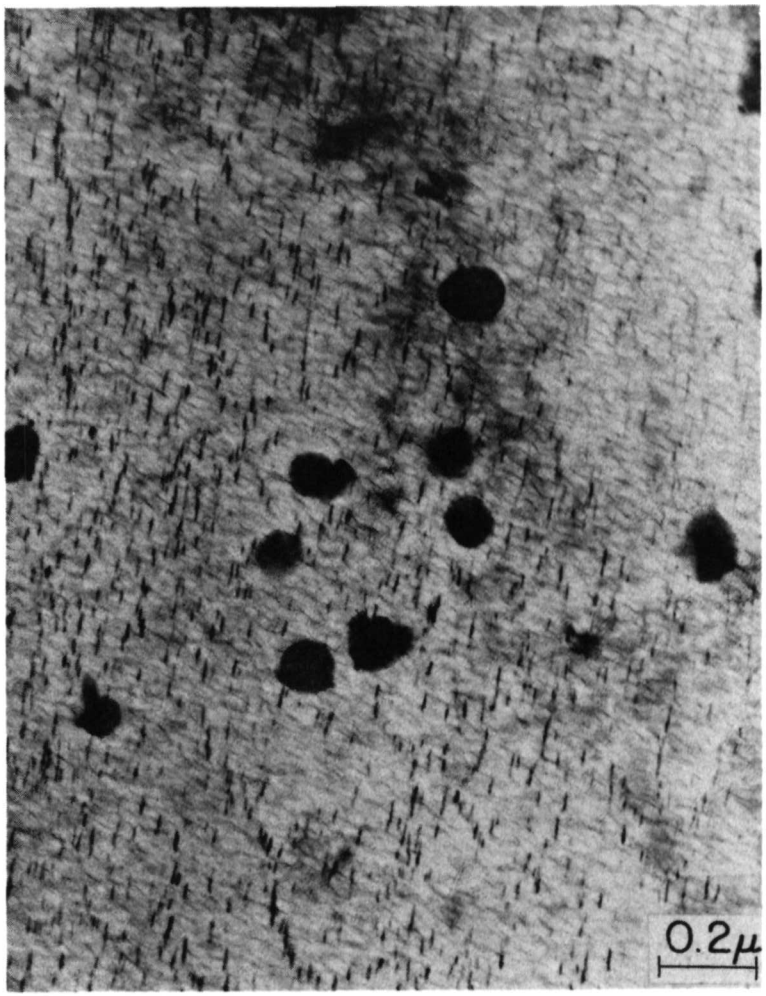

Fig. 16 Transmission Electron Micrograph Showing Dispersed Particles and Hardening Precipitates

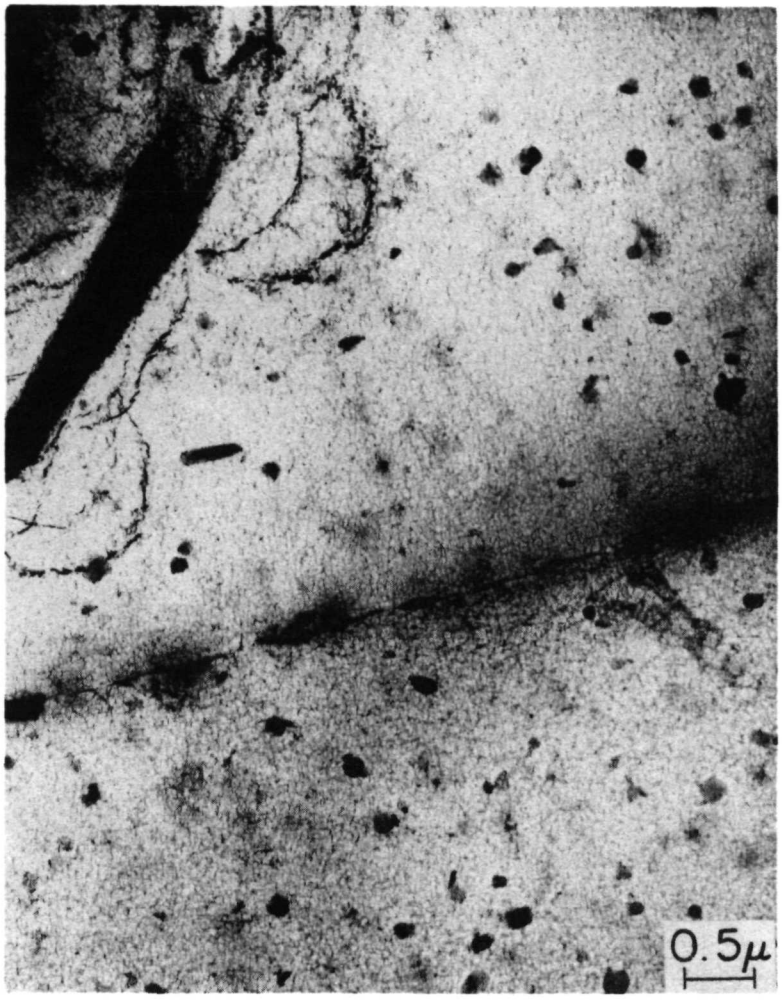

Fig. 17 Transmission Electron Micrograph Showing Small Inclusions at Grain Boundaries

is possible even if no precipitation free zone exists. If inclusions lie along grain boundaries and either are at small distances between each other, or nucleate cavities before the randomly distributed inclusions, a dimpled topography should show in the fractographs as a result of void growth and coalescence at these inclusions. In this case, the dimples should not be shallow (i.e. approximately of the thickness of the precipitation free zone, as those found by Ryder and Smale[5]), and therefore may be difficult to distinguish from dimples formed at the randomly distributed particles found in the matrix.

IDENTIFICATION OF VOID-NUCLEATING PARTICLES

Since the largest part of the fracture surface was covered by large dimples, the large inclusions, believed to be responsible for them, probably control the toughness of the alloy. It is therefore necessary to determine the elements present in these and, if possible, their specific composition.

Polished samples, in which inclusions were easily seen in the optical microscope, were first analysed to determine the elements present in all of the large inclusions. Figure 18 shows typical micrographs obtained with the micro probe analyser. The top left picture shows the sample current by which it is possible to show the location of the particles. The remaining picture show the distribution of each of the specific elements investigated. Particles containing Fe, Mn and some Si are found in general, together with some particles containing large amounts of Cu. In these polished-section micrographs, it is not possible to decide if the particles contained Al because of interference from the Al matrix.

Extraction replicas of the fracture surface were then analysed to compare with these results on polished surfaces (a description of the technique used to extract the particles is found in the appendix). Figures 19 and 20 show

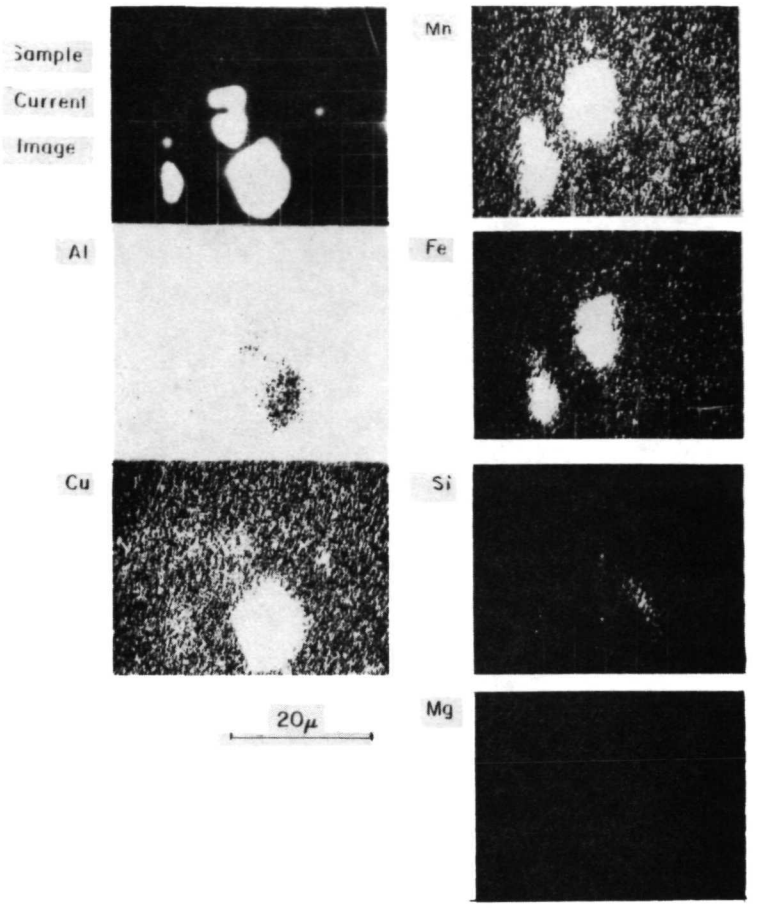

Fig. 18 Electron Micro Probe Analysis of a Polished Sample of the Alloy

electron micrographs of typical extraction replicas. Many particles were extracted and seem to remain in the place corresponding to the dimple they had originated. However, some were found moved from their original position. The micro probe showed that the particles contained Cu, Si and Al, and some only Si, Figure 21. Comparing these results with those of the polished samples, it seems that either the particles containing Fe, Si and Mn were not extracted from the fracture surface or that they do not contribute to the formation of dimples. Direct micro probe analysis of the fracture surface with the micro probe, which detected the inclusions which contained Fe, and the fact that no special type of inclusions was found not to crack in the deformed samples seems to indicate that the inclusions were not extracted from the fracture surface.

The composition of the particles containing Fe, Mn and Si was estimated by comparing the intensity of the micro probe X-rays of the specific elements.

The estimated composition of these particles is shown in Table III together with that of a possible intermetallic phase [8]. The agreement is reasonable.

Table III

Micro probe Estimate of
Chemical Composition of Mn-Fe-Al-Si Type Particle (wt.-pct.)

Mn	Fe	Si	Al
12~13	8~10	3~4	$\geq$ 50

Chemical Composition of:			
	Mn	Fe	Si	Al
$Al_{12}(FeMn)_3Si$	32		5	63

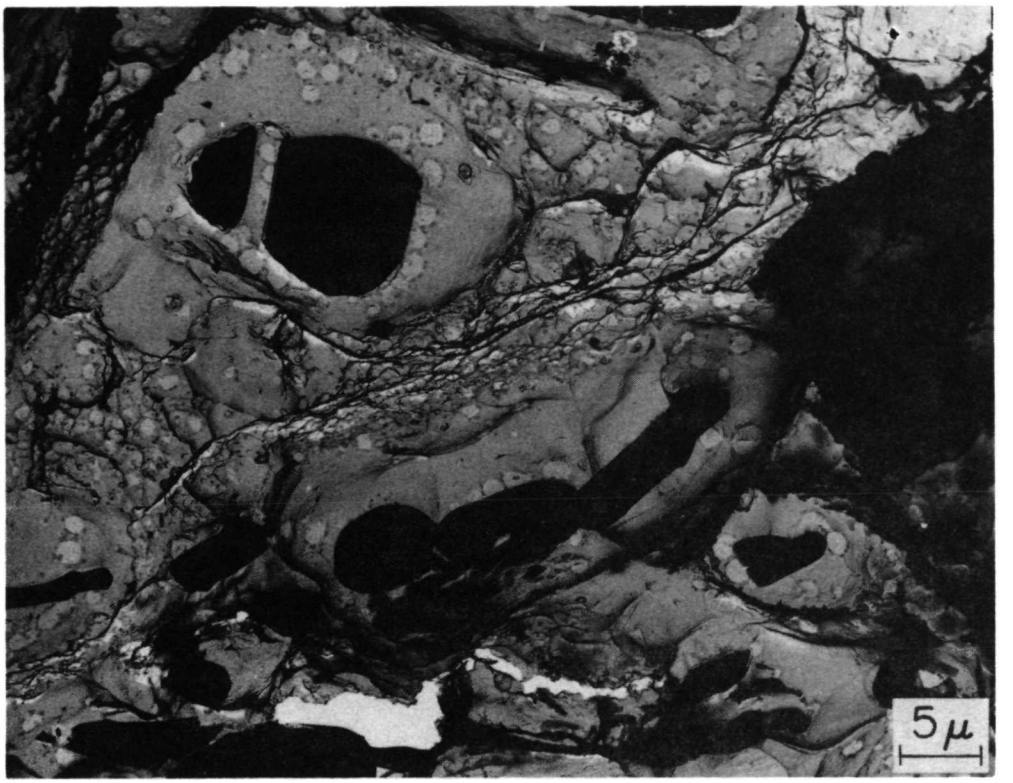

Fig. 19 Electron Microscope Micrograph of an Extraction Replica

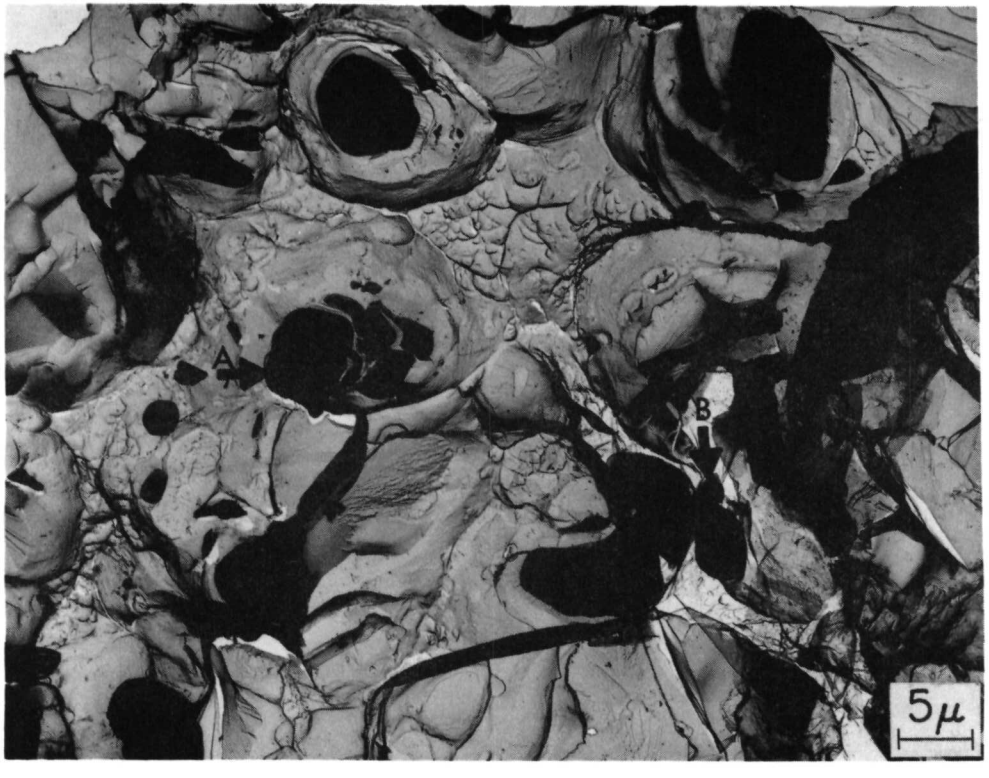

Fig. 20 Electron Microscope Micrograph of an Extraction Replica

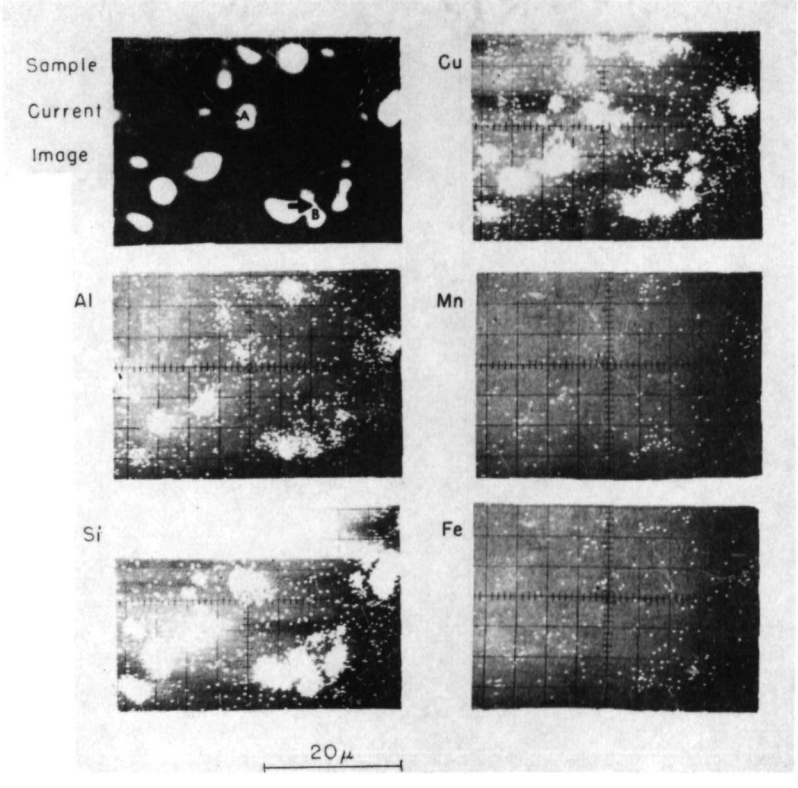

Fig. 21 Electron Micro Probe Analysis of Particles in Extraction Replica Shown in Fig. 20

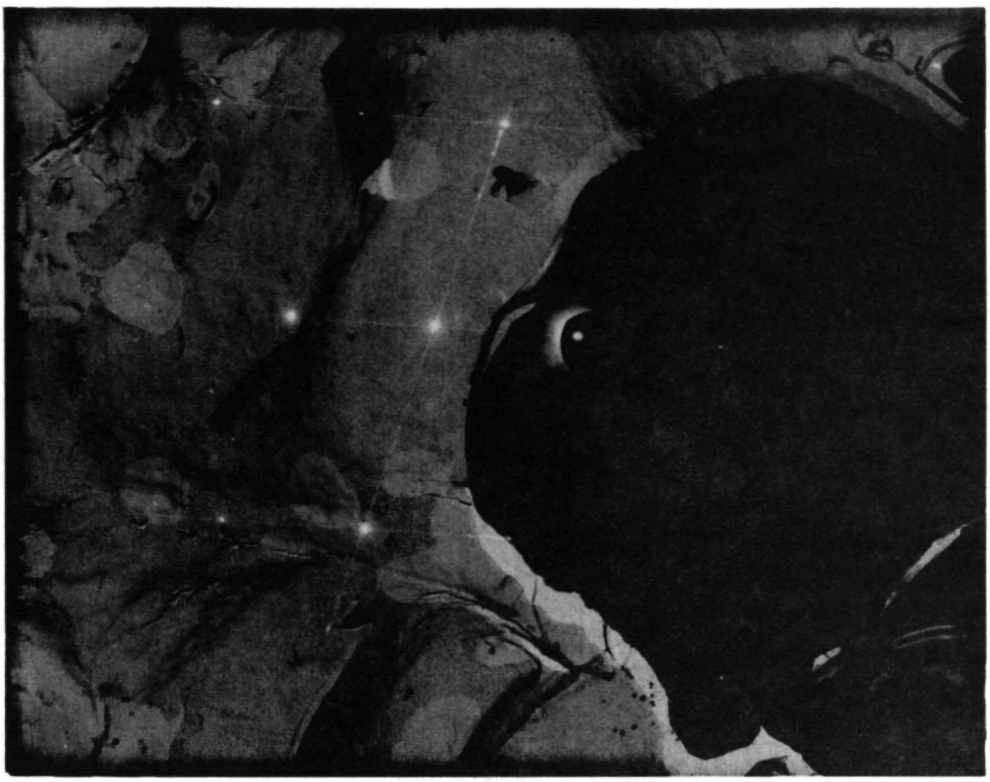

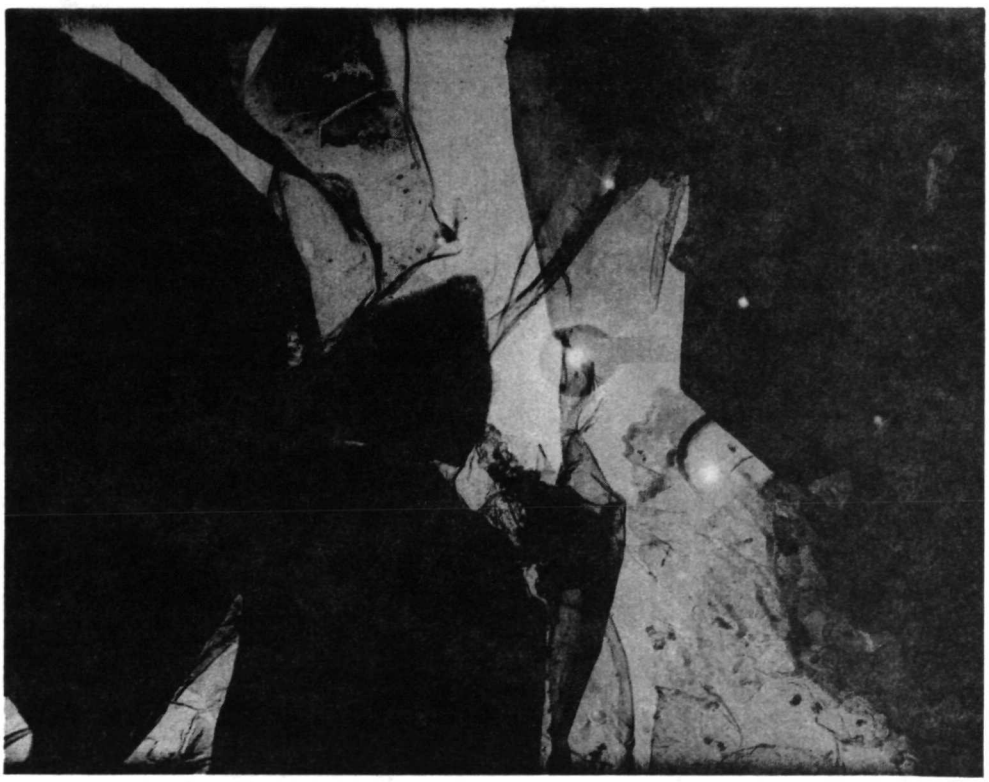

Fig. 22 a & b Electron Diffraction Patterns of Particles A and B of Fig. 20

For the particles containing Cu, it was possible to obtain electron diffraction patterns whenever they appeared thin enough in the extraction replicas. Figures 22a and b shows diffraction patterns for the particles A and B shown in Figure 20 and in the micro probe micrograph in Figure 21. An analysis of the diffraction patterns obtained of the particles in the extraction replicas might correspond to Al_4Cu_9 or $Cu_{15}Si_4$ and pure Si or Cu_5Si or $CuAl_2$.

We may therefore conclude that two varieties of large particles are found in the alloy. One, which has been estimated to be very likely $Al_{12}(FeMn)_3Si$, corresponds to the inclusions which in the optical micrographs appeared with a more irregular form and a darker grey. The other type, which correspond to the more equiaxed, lighter colored particle in the optical micrographs, does not contain Fe or Mn, and contains Al and Si combined with Cu and possibly Mg since Mg was not included in the micro probe analysis of these extracted particles.

FRACTOGRAPHIC OBSERVATION OF THE BOUNDARY BETWEEN FATIGUE CRACK AND DIMPLED RUPTURE REGIONS OF FRACTURE SURFACE

Figure 23 shows an electron fractograph taken from a two stage plastic-carbon replica made at the boundary between the fatigue (F) and the dimpled ruptures(D) regions of the fracture surface. The fatigue region in this material does not show the striations typical of fatigue. However, the features of the dimpled rupture region are quite different from these of the fatigue region which may be seen more clearly in a low magnification fractograph taken with the scanning electron microscope, Figure 24.

Fig. 23 Electron Microscope Micrograph of a Two Stage Replica of the Boundary Between Fatigue (F) and Overload Region (D).

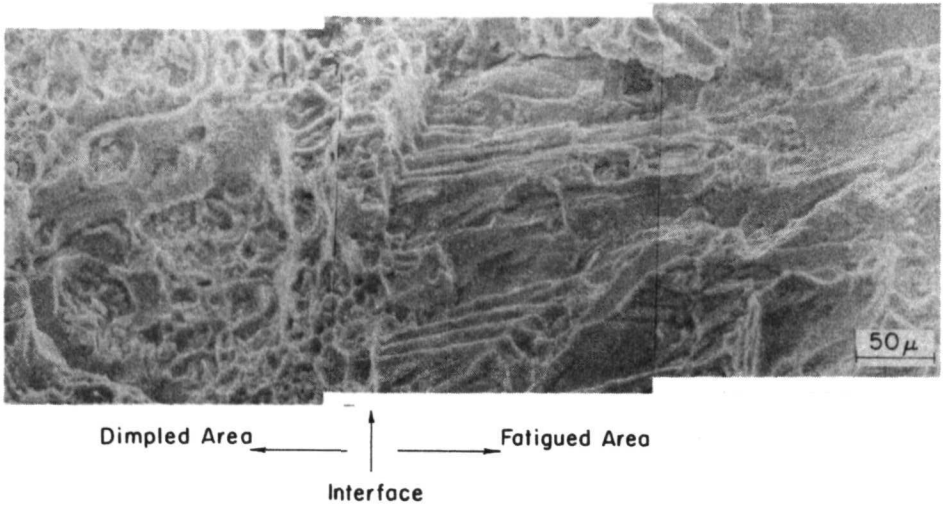

Fig. 24 Low Magnification Electron Micrograph Taken With the Scanning Electron Microscope of an Area Similar to that in Fig. 23

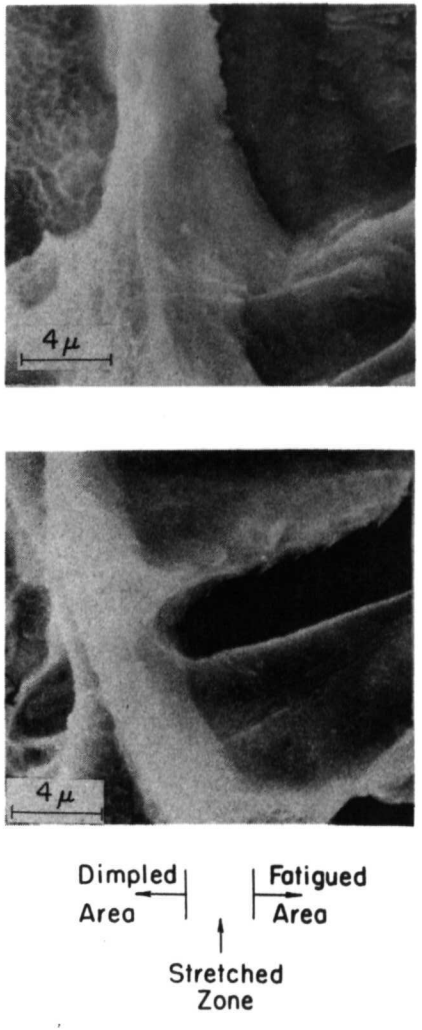

Fig. 25 High Magnification of Areas in Fig. 24 at the Boundary

At the boundary between the two regions, a step may be seen, Figure 24, which does not appear clearly in replicas due perhaps to collapse of the carbon film which will not support such a step. In any event, a topography different from both the dimpled rupture and the fatigue region is seen at the boundary, (shown between arrows) Figure 23. This transition area has been called the stretched-zone[13] and its topography of the surface is said to be made up of almost wholly of "serpentine glide" due to slip[10]. It is apparent from Figure 23 that the extent of this region is quite irregular. Two scanning electron micrographs at higher magnification of the stretched zone are seen in Figure 25. The step seen at lower magnification in Figure 24 now appears to be rounded. The sketch shown in Figure 26 shows, we believe, the situation at the tip of the crack just before critical instability. We therefore believe that the stretched zone is produced during blunting of the crack tip and perhaps some stable crack growth. Several correlations have been made recently between the size of the stretched zone and fracture mechanics data. The result seems to be that the size of the stretched zone is of the order of $G_{Ic}/4\sigma_y$, where G_{Ic} is the critical crack extension force and σ_y the yield stress[11]. If we take $G_{Ic}/2\sigma_y$ as a measure of the "crack opening displacement" (COD) at instability (the factor 1/2 is used when considering plane strain conditions)[14], then, roughly, the radius at the tip of the crack just before instability is of the order of one-half to one times the crack-opening-displacement in size.

The formation of the stretched zone must involve some complex slip mechanism at the crack tip. We would like to suggest here that this mechanism should be similar to that proposed by Rogers[12] to explain the formation of lips of a ductile copper tensile specimen that failed in a double cup fashion. The mechanism has been called "ductile cutting." Two factors, which we believe are also involved in the formation of the stretched zone are large amounts of plastic deformation necessary to provide the separation or "cutting" of the material and low triaxiality to inhibit void growth during its formation.

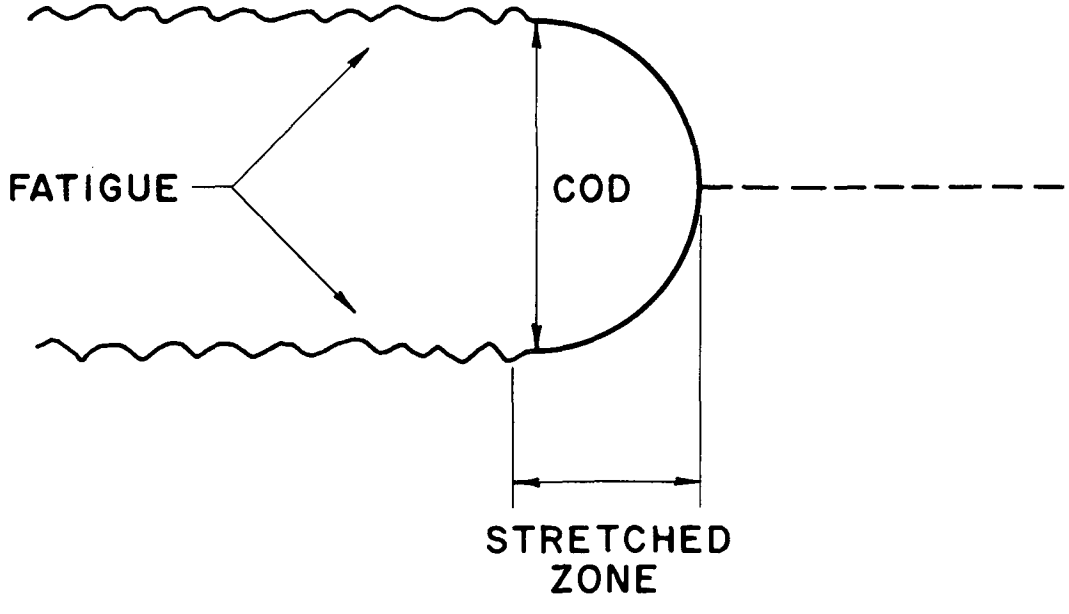

Fig. 26 Sketch Showing Blunting of the Crack Tip and the Stretched Zone

DISCUSSION

From the fractographic study made of the fractured toughness specimens of the alloy, several conclusions may be drawn.

The geometrical correlation between size and distribution of large dimples and the size and distribution of the large particles readily seen in the optical microscope made it apparent from the beginning that these inclusions are responsible for the nucleation of voids leading to the large dimples. Further evidence is provided by the extraction replicas in which it was possible to relate in many cases a large dimple with its nucleating inclusion. Although it was not possible to extract the inclusions containing Fe, Mn and Si, direct micro probe analysis of the fracture surface, and the fact that they were found to fracture in the deformed tensile specimens, showed that these inclusions were also responsible for the large dimples.

These large dimples cover more than 50% of the fracture surface and hence the inclusions which have acted as nuclei of the voids must be significantly reducing the toughness of the material.

In general, voids are nucleated by fracture of the inclusions, and as already mentioned all large inclusions, regardless of type were observed to crack in the tensile deformation experiments, suggesting indirectly that all of the large inclusions were nucleating cavities. Around 10% of the particles were found cracked at strains of 3% and 45% at strains of about 5%. It is very likely then that almost all of the inclusions within the plastic zone at the tip of the crack of the toughness specimens were cracked well before the unstable fracture started. Most of the rest of the fracture process leading to the critical instability must have been growth of these cavities through the matrix and coalescence with other cavities.

The fractographs seem to show a situation by which several voids nucleated at large particles coalesce somewhat at the same level and parallel to the main fracture surface. Thereafter they join with other similar areas by a mechanism of void sheet formation[9] leading to the rupture of the ligament between these areas. The void sheet formation mechanism seems to be developed through the formation of voids at small particles distributed uniformly in the matrix, or in some cases, at the small inclusions found at the grain boundaries. It is difficult to distinguish the areas covered by small dimples which are related to grain boundaries and those which are not. However, features such as the one seen in Figure 14, could well be related to grain boundary failure.

CONCLUSIONS

1. All of the fractographic evidence indicates that the fracture process is dominated by cavity nucleation, caused by fracture of the large impurity inclusions tentatively identified as $Al_{12}(Fe, Mn)_3$ Si and a combination of excess Cu with either Al, Si or Mg.

2. From their size and distribution, it is unlikely that these large inclusions contribute to the strength of the alloy and presumably greatly decrease its fracture toughness.

3. These first two conclusions suggest that modification of the composition to reduce the density of the two major types of large inclusions should bring about an improvement in fracture toughness without significant loss of strength.

4. These conclusions should be tested by making up a 2014 alloy, with its composition so modified as to eliminate or minimize the number of these two types of inclusions and testing its strength and fracture toughness after a suitable heat treatment.

APPENDIX

Development of the Technique to Extract Inclusions From the Fracture Surfaces

Attempts to extract inclusions from the fracture surface, either by two stage plastic-carbon replication or by direct carbon replication, indicated the particles were tightly bound to the matrix and could not be extracted readily by either method. In the direct carbon case, removal of the carbon film and the inclusions was attempted by electropolishing the surface that had been carbon shadowed, in a solution of percloric acid and ethanol, with 10 volts applied between cathode and anode.

An oxide replica technique developed by Keller and Geisler[7] was then tried with negative results. A film of aluminum oxide was produced on the fracture surface by anodic oxidation in a solution of 48 gr. hydrophosphate, 2ml. sulphuric acid and 400ml water. 20 to 40 volts were applied during 3 to 5 minutes. After the oxidation the fracture surface was scored with a razor blade, into small squares of roughly the size of the grids to be used in the electron microscope (3mm diameter), and immersed in a solution of mercuric chloride. The roughness of the fracture surface and irregularity of the thickness of the oxide film seemed to make it impossible to obtain any good pieces of oxide to be examined in the electron microscope.

The next technique used was a plastic-carbon replica applied after electro-etching in a solution of 1/3 nitric acid 2/3 methanol at -25°C. The result was that some particles were extracted but seemed to lose their relation to the dimple where they had been on the fracture surface.

Finally it was found that the best technique was a direct carbon replica with pre-etching before depositing the carbon. The specimen was electro etched with the same nitric acid-methanol solution as before, by applying a voltage of 0.5V for 30 seconds and left without voltage for an extra 60 seconds. After carbon deposition the surface was coated with a special wax (Ladd Laboratories) which was melted and then poured over the carbon-coated fracture surface. Scoring the surface into small squares and electro-polishing with 10.5 volts at -25°C freed the small squares which then floated on the surface of the solution. After retrieving the replica fragments from the solution the wax was removed by soaking the fragments in xylene. By this method it was frequently possible to extract non-metallic particles from the fracture surface and, as shown in Figures 19 and 20, retain them in position with respect to the dimples which they nucleated. The method successfully extracted the inclusions containing Cu, Si and Al but failed to extract those containing Fe, Mn and Si.

REFERENCES

1. J. R. Low, Jr., Engr. Fract. Mech., 1, 47, (1968)
2. J. G. Kaufman and M. Holt, Alcoa Res. Labs. Tech. Paper N° 18 (1965)
3. R. D. Schoone and E. A. Fiscione, Rev. of Scient. Instr. 37, 1351, (1966)
4. M. F. Ashby in "Strengthening Methods in Crystals," Ed. A. Kelly and R. B. Nicholson, Elsevier (1969)
5. D. A. Ryder and A. C. Smale in Fracture of Solids, p. 237, Interscience N. Y. (1963)
6. G. Phragmen, J. Inst. Metals 77, 489 (1950)
7. F. Keller and A. H. Geisler, Trans. AIME 156, 82, (1944)
8. W. A. Anderson, Aluminum Company of America, private communication
9. H. Rogers in "Ductility," ASM seminar, (1968)
10. C. D. Beachman and D. A. Meyn, N. R. L. Memorandum Report 1547 (1964)
11. A. Brothers, ASTM Task Group of E-24, Philadelphia meeting March 1969
12. H. Rogers, Trans. AIME 218, 498, (1960)
13. U. E. Wolff, Reactor Primary Coolant System Rupture Study, AEC Research and Development Report GEAP-5474, Jan. 1967
14. G. Irwin, private communication